Water ADC, Extracellular Space Volume, and Tortuosity in the Rat Cortex After Traumatic Injury

I. Voříšek,[1,3] M. Hájek,[2,3] J. Tintěra,[2] K. Nicolay,[4] and E. Syková[1,3,5]*

The diffusion parameters in rat cortex were studied 3–35 days following a cortical stab wound, using diffusion-weighted MR to determine the apparent diffusion coefficient of water (ADC$_W$) in the tissue, and the real-time iontophoretic tetramethylammonium (TMA) method to measure the extracellular space (ECS) diffusion parameters: ECS volume fraction α and the ADC of TMA$^+$ (ADC$_{TMA}$). Severe astrogliosis was found close to the wound, and mild astrogliosis was found in the ipsilateral but not the contralateral cortex. Chondroitin sulfate proteoglycan (CSPG) expression was increased throughout the ipsilateral cortex. In the hemisphere contralateral to the wound, α, ADC$_{TMA}$, and ADC$_W$ were not significantly different from control values. ECS volume fraction was increased only in the vicinity of the wound, in the region of cell death and severe astrogliosis, at 3 and 7 days after injury. However, both ADC$_{TMA}$ and ADC$_W$ were significantly decreased after lesion in the vicinity of the wound as well as in the rest of the ipsilateral hemisphere distant from the wound. Thus, both ADC$_W$ and ADC$_{TMA}$ decreased in regions wherein α did not change but CSPG increased. An increase in extracellular matrix expression may therefore impose diffusion barriers for water as well as for TMA molecules. Magn Reson Med 48:994–1003, 2002. © 2002 Wiley-Liss, Inc.

Key words: apparent diffusion coefficient; astrocytes; chondroitin sulfate proteoglycan; extracellular matrix; cell swelling

Reactive gliosis is a common phenomenon in the central nervous system (CNS) following a loss of neurons during different neurological disorders and after brain injury. Astrogliosis is characterized by astrocyte proliferation; extensive hypertrophy of nuclei, cell bodies, and processes; and increased expression of glial fibrillary acidic protein (GFAP). The hypertrophied reactive astrocytes, in most cases, form a glial scar. A stab wound of the rodent brain is the most common model of reactive gliosis (1). Our earlier work demonstrated that astrogliosis around the stab wound could impose additional diffusion barriers in the CNS (2) due to the hypertrophy of astrocytic processes and the increased production of extracellular matrix components such as chondroitin-sulfate proteoglycan (CSPG). The morphology and immunohistochemistry of neural tissue around stab wounds have been extensively studied (1,3–8). Increased CSPG expression was observed following puncture lesions of the rat cerebellum (9) and transection of the rat brain postcommisural fornix (10). The dynamic properties of CSPG and perineuronal nets in the rat brain were investigated by Brückner et al. (11).

In a previous study (2) the diffusion properties in the close vicinity of a stab wound were investigated using the real-time iontophoretic tetramethylammonium (TMA) method. That study revealed that the increase in extracellular space (ECS) volume fraction and tortuosity observed following wounding is related to astrogliosis and an increase in extracelluar CSPG. In the present study we employed two methods to compare their sensitivity to diffusion changes in the rat cortex after injury, extending our measurements to cortical areas distant from the wound and to the contralateral hemisphere. We examined the diffusion properties of the rat cortex after a cortical stab wound using the real-time iontophoretic tetramethylammonium (TMA) method (12,13) and diffusion-weighted ^{1}H magnetic resonance imaging (DW-MRI). The TMA method determines the apparent diffusion coefficient of TMA$^+$ (ADC$_{TMA}$) in the extracellular space. In addition, this method also determines the ECS volume fraction α (α = ECS volume/total tissue volume) and the nonspecific cellular uptake of TMA (k'). The TMA method is based on monitoring the diffusion of the small TMA$^+$ cation (molecular weight = 74) to which cell membranes are practically impermeable, i.e., TMA$^+$ applied extracellularly diffuses predominantly in the ECS. The local concentration of TMA$^+$ following its iontophoretic application can be measured in vivo using ion-selective microelectrodes (for review, see Refs. 14 and 15). The diffusion properties of TMA$^+$ are comparable to those of many neurotransmitters (e.g., acetylcholine, γ-aminobutyric acid, and glutamate). DW-MRI determines an ADC of water (ADC$_W$) in the tissue, which receives contributions from the diffusion characteristics of both the extra- and intracellular space (16). ADC$_W$ and ADC$_{TMA}$ were therefore studied 3–35 days post-lesion and compared with the changes in α. Following TMA and MR measurements, the changes in extracellular matrix and astrogliosis were determined by immunohistochemical staining for CSPG and GFAP.

The aim of the study was to determine whether a decrease in ADC$_W$ is related to a decrease in ECS volume fraction around the wound, or whether diffusion barriers imposed upon TMA molecules diffusing extracellularly can also decrease ADC$_W$. In our stab-wound model, we can study the diffusion parameters either in the vicinity of the wound, where α is increased, or in the rest of the ipsilateral hemisphere, where α is not changed but ADC$_{TMA}$

decreases due to additional diffusion barriers resulting from astrogliosis or increased extracellular matrix expression [2].

METHODS

Experimental Animals

Experiments were performed on male rats (Wistar strain), 2.5–3 months old, with body weights of 260–340 g. A unilateral sterile cut through the cortex was made as an experimental model of traumatic injury [1]. Part of the skull was unilaterally removed with a dental drill, and a fine microdissecting knife was used to make a stab wound 4 mm long and 2 mm deep, −1.5 mm caudal from the bregma and 2 mm from the midline [17]. Care was taken not to cut the corpus callosum. The skin overlying the cranium was sutured. The TMA and MR diffusion measurements were performed in the cortex on days 3 and 7 post-wounding and once during the 21–35 days post-wound.

Before the stab-wounding and TMA measurements, the animals were anesthetized by an intraperitoneal injection of sodium pentobarbital (60 mg/kg), and anesthesia was maintained by injection of 15 mg/kg approximately every 60 min. The animals spontaneously breathed air. The head of the animal was fixed in a stereotaxic apparatus. The cranial bones and the dura mater were carefully removed above the regions selected for TMA measurements. The exposed brain tissue was bathed in warm (37°C) artificial cerebrospinal fluid [18]. Microelectrodes were introduced into the brain cortex using a remote control micromanipulator (Nanostepper, SPI, Germany). The stereotaxic coordinates were bregma −3.4 mm and either 2.3–4.0 mm lateral for measurements in the somatosensory cortex or 6 mm lateral for measurements in the auditory cortex [17].

During MR measurements, halothane was used as an inhalation anesthesia at a maintenance concentration of 1–2%. The rats were intubated 5 min after premedication consisting of a subcutaneous injection of 1.0 ml/kg Hypnorm® (10 mg/ml fluanisone + 0.315 mg/ml fentanyl citrate) and 1.0 ml/kg Dormicum® (5 mg/ml midazolam) (Jansen Animal Health, Belgium). The animals breathed a mixture of oxygen (30%) and nitrous oxide (70%), supported by an animal ventilator. The breathing frequency was maintained at 30 breaths/min with a 1:1 inspiration : expiration ratio, and the CO_2 level in the expired air was monitored. Throughout the MR measurements, the animals were fixed in a nonmagnetic head-holder. The body temperature of the rats was monitored by a rectal temperature probe and maintained during the whole period of TMA and MR measurements at 37°C by means of a heating pad. When the directional dependence of the ADC in the cortex of control animals was measured, a similar experimental protocol was used with a few minor differences. For inhalation anesthesia, isoflurane was used at a maintenance level of 1.5%, and the breathing frequency was maintained at 50 breaths/min. Blood oxygenation was monitored instead of CO_2 concentration in the expired air.

The animal experiments performed in this study were carried out in accordance with all institutional and national regulations, and the European Communities Council Directive of 24 November 1986 (86/609/EEC).

TMA⁺ Measurements of ECS Diffusion Parameters

Ion-selective microelectrodes (ISMs) for the measurement of TMA⁺ diffusion parameters in the ECS were prepared as described previously [19]; the ion-exchanger was Corning 477317, and the ion-sensing barrel was back-filled with 100 mM TMA chloride instead of 150 mM KCl. Electrodes were calibrated using the fixed-interference method before and after each experiment in a sequence of solutions of 150 mM NaCl + 3 mM KCl with the addition of the following concentrations of TMA chloride: 0.0003, 0.001, 0.003, 0.01, 0.03, 0.1, 0.3, 1.0, 3.0, and 10.0 mM.

For diffusion measurements, iontophoresis pipettes were prepared from theta glass (Clark Electrochemical Instruments, Pangbourne, UK). The shank was bent before it was back-filled with 0.5 M TMA chloride so that it could be aligned parallel to the ion-selective microelectrode. The electrode arrays were prepared by gluing together an ion-selective microelectrode and two iontophoresis pipettes with a tip separation of 110–180 μm (Fig. 1). The tips of the pipettes formed a 90° angle (see Fig. 1) in the horizontal or vertical planes, which allowed for quasi-simultaneous measurements in perpendicular directions. Typical iontophoresis parameters were +20 nA bias current (continuously applied to maintain a constant transport number), with a +80 nA current step of 60 s duration to generate the diffusion curve. The reference electrode–Ag/AgCl wire was placed in the muscle. Potentials recorded on the reference barrel of the ISM were subtracted from the ion-selective barrel voltage measurements by means of buffer and subtraction amplifiers.

Concentration-vs.-time curves for TMA⁺ diffusion were first recorded in 0.3% agar gel (Special Noble Agar; Difco) made up in a solution of 150 mM NaCl, 3 mM KCl, and 1 mM TMA in a Lucite cup placed just above the brain. The array of electrodes was then slowly lowered into the cortex to appropriate depths. The measurements were done in 200-μm steps, in the vicinity of the wound (300–1000 μm laterally from the wound), at a distance of 1500–2000 μm from the wound, and in the auditory cortex (Au). Diffusion curves were recorded at the wound site and also at corresponding places in the contralateral hemisphere of lesioned animals (see Fig. 1). The data were compared with measurements performed simultaneously on intact animals, as well as with previously published measurements [20,21].

Diffusion curves obtained in agar gel were analyzed using the program VOLTORO (C. Nicholson, unpublished). They were fitted by a SIMPLEX algorithm according to the diffusion equation [19] in order to determine the transport number (n) of the iontophoretic micropipette. After determining n in agar gel, measurements were made in the brain to obtain α, ADC_{TMA}, and k'. ADC is a tensor and incorporates six independent components. With the TMA method, we were able to determine its diagonal components (ADC_x, ADC_y, and ADC_z). The measurements, of course, are extremely sensitive to the orientation of the object in the measurement apparatus, and we therefore positioned the animals in the stereotactic frame in exactly the same way for every experiment. The diffusion parameters were calculated from the concentration-vs.-time profiles by fitting Eq. [1] and similar equations for the other
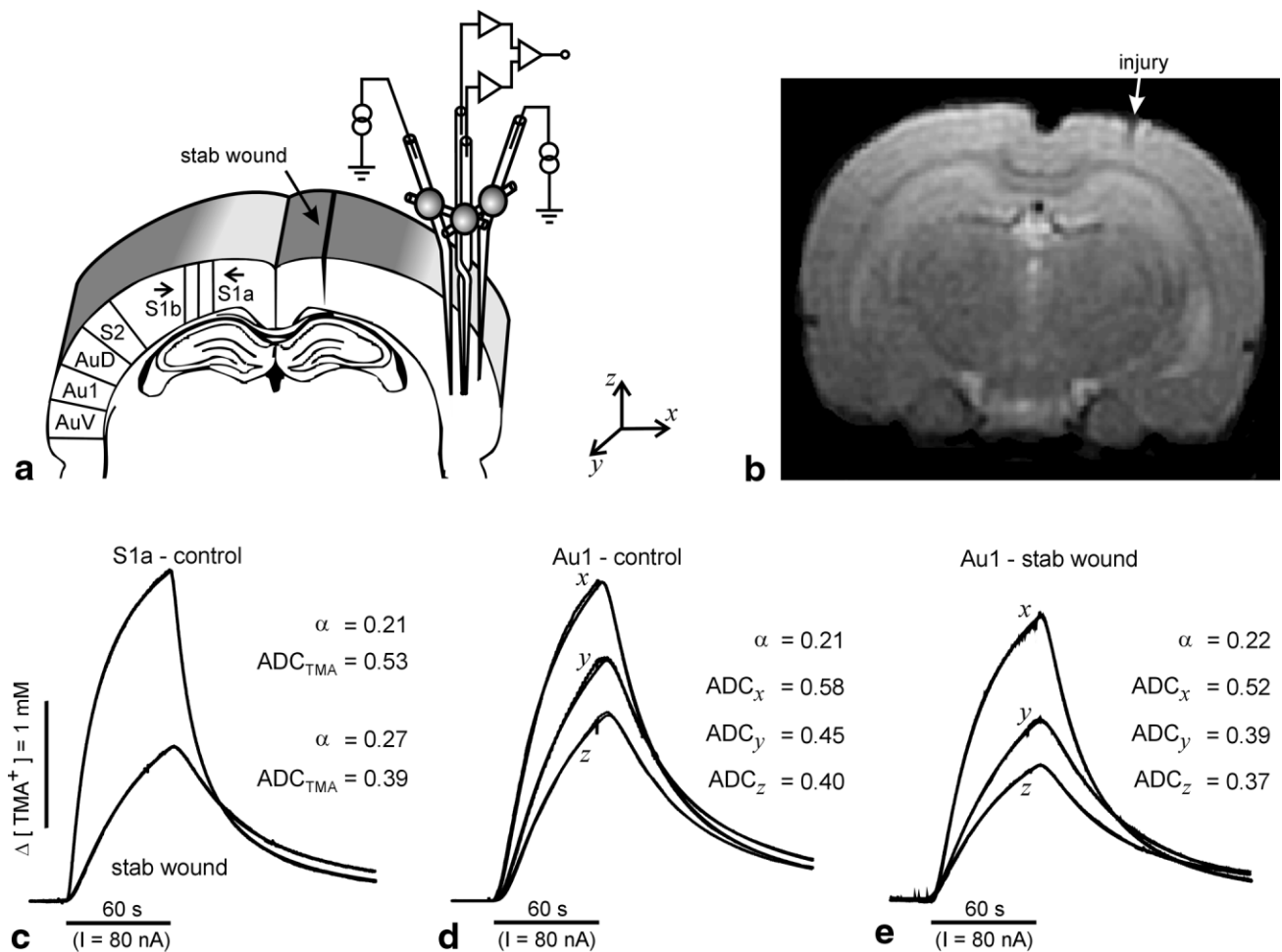
FIG. 1. **a:** The experimental arrangement for diffusion measurements. A current pulse released TMA$^+$ ions into the tissue from an iontophoretic micropipette. The resulting changes in TMA$^+$ concentration were recorded with an ion-selective microelectrode in the form of diffusion curves. **b:** T_2-weighted image showing the localization of the wound. **c:** Typical diffusion curves and the corresponding diffusion parameters from the S1 region. The higher curve was recorded in the cortex of a control animal, while the smaller curve indicates the restricted diffusion in the vicinity of the wound (S1a region) 7 days after injury. The horizontal bar below the curves represents the duration of the iontophoretic pulse. **d** and **e:** Representative records from the auditory cortex (**d**) before and (**e**) after stab wound. To reveal possible diffusion anisotropy, measurements were performed in the Au1 along three perpendicular axes: *x*, *y*, and *z*. The tips of two iotophoretic micropipettes and the ion-selective microelectrode formed a 90° angle for simultaneous measurements along the *x*- and *y*-axes (also along the *x*- and *z*-axes or the *y*- and *z*-axes). The theoretical data curve is superimposed on each diffusion curve. The shape and amplitude of the diffusion curves reflect the different diffusion coefficients along each of the selected axes. The ADC units are $\times$ 10^{-5} cm^{2}s^1.

axes with VOLTORO. The axes for ADC$_{TMA}$ measurement (hereafter called the "laboratory coordinates") were chosen along the mediolateral direction (*x*), the rostrocaudal direction (*y*), and the dorsoventral direction (*z*). The experimental arrangement and axes orientation are shown in Fig. 1.

The expected extracellular TMA$^+$ concentration, *C*, generated by iontophoresis in a homogeneous and potentially anisotropic medium was derived by Rice et al. (22) as follows: When the iontophoretic pulse is applied for duration *d*, then $C = G(t)$ for the rising phase of the curve ($t < d$), and $C = G(t) - G(t-d)$ for the falling phase of the curve ($t \geq d$). For measurements performed along the coordinates (*x*, 0, 0) relative to the iontophoretic electrode at the origin (0, 0, 0), the expression of function $G(u)$ can be given as:

$$G_x(u) = QA_x/8\pi x[\exp(x\sqrt{k'/ADC_x})\mathrm{erfc}(x/2\sqrt{uADC_x}$$
$$+ \sqrt{k'u}) + \exp(-x\sqrt{k'/ADC_x})\mathrm{erfc}(x/2\sqrt{uADC_x} - \sqrt{k'u})] \qquad [1]$$

where

$$1/A_x = \alpha ADC_z ADC_y. \qquad [2]$$

A similar expression can be written down for measurements along the *y*- and *z*- axes. The source $Q = In/zF$ (*I* is the current applied to the iontophoretic electrode, *n* is the transport number of this electrode, *z* is the number of elementary charges on the ion, and *F* is Faraday's electrochemical equivalent). Nonspecific concentration-depen-

dent uptake is k' (12,23,24) and "erfc" is the complementary error function. The value of α could be calculated using Eq. [2] with averaged experimental data from each axis, and similar expressions for the other components. The three estimates of α and k' obtained with this method were averaged to yield the values that represent α and k' in the homogeneous region in which the measurements were performed. If the coordinate system is chosen properly with respect to brain structure, diffusion anisotropy can be fully characterized by the three components of ADC_{TMA}, here designated as ADC_x, ADC_y, and ADC_z. If there was no statistically significant difference among the parameters ADC_x, ADC_y, and ADC_z, the region was classified as isotropic.

MR Measurements of Water ADCs

The DW-MRI measurements of wounded and control animals were performed using an experimental MR spectrometer (4.7 T; Varian, INOVA) (40-cm Oxford magnet), equipped with a gradient system (220 mT/m, 300 μs rise time) and a 10-cm resonator with a 2-cm inductively coupled surface coil. Twenty-one T_2-weighted coronal images (TE = 60 ms, TR = 3 s, two acquisitions, field of view (FOV) = 3×3 cm^2, matrix size = 256×128, slice thickness = 1 mm) were measured in order to localize a slice of interest. Ten coronal DW images were measured using a spin-echo sequence in each rat brain with the following parameters: gradient pulse duration δ = 6 ms, gradient orientated along z axis (rostral–caudal direction), the time between the rising edges of the diffusion-encoding gradients was kept at Δ = 19 ms; b-factors = 132, 598, and 1294 s/mm^2; TE = 33 ms; TR = 3 s; FOV = 3×3 cm^2; matrix size = 256×128; slice thickness = 1 mm; and slice separation = 0 mm.

To reveal presumed ADC_W anisotropy in the cortex, additional measurements were performed in normal, non-lesioned rats. A BIOSPEC 4.7 T system (Bruker, Germany) equipped with a 200 mT/m gradient system (190 μs rise time) and a head surface coil was used to acquire 11 T_2-weighted sagittal images (TE = 20 ms, TR = 1.5 s, four acquisitions, FOV = 3.84×3.84 cm^2, matrix size = 256×128, slice thickness = 1 mm) and six DW images per slice in each one of the diffusion-encoding gradient directions (Δ = 30 ms; b-factors = 66, 251, 589, 943, 1382, and 1723 s/mm^2; TE = 45 ms; TR = 1200 ms; FOV = 3.84×3.84 cm^2; matrix size = 256×128; four 1-mm-thick coronal slices; slice separation = 0.5 mm). DW images were measured using the stimulated echo sequence. The diffusion gradient direction pointed along the x (phase direction), y (slice direction), and z (read direction) axes (Fig. 1) and in mixed directions (read-slice, read-phase, phase-slice, and read-phase-slice). The slices were acquired interleaved. The cross-term factors were taken into account for b-value enumeration. The comparability of ADC values measured along different axes was verified by means of five diffusion phantoms placed on the top of the rat's head. The phantoms were made from glass tubes (inner diameter = 2.3 mm; glass type: KS80; Rückl Glass, Czech Republic) filled with pure (99%) substances with different diffusion coefficients. The substances were 1-octanol, n-undecane (Sigma Aldrich, Czech Republic), isopropyl alcohol,

n-butanol, and tert-butanol (Penta, Czech Republic). The temperature of the phantoms was maintained at a constant 37°C. For all MR measurements we used the same coordinate framework (laboratory coordinates) as for the TMA measurements, which was different from that commonly used in the MR field (y- and z-axes were transposed).

Immunohistochemistry

Following both MR and TMA diffusion measurements, the anesthetized animals were perfused through the heart with 4% paraformaldehyde in 0.1 M phosphate-buffered saline (PBS, pH 7.5). Fixed brains were dissected out and immersed in PBS with 30% sucrose. Frozen coronal sections (40 μm) were cut through the areas of interest. Astrocytes were identified using monoclonal antibodies to glial fibrillary acidic protein (GFAP) (Boehringer-Mannheim, Mannheim, Germany). Immunostaining for CSPG was done using monoclonal anti-chondroitin-sulfate CS-56 antibody (Sigma Aldrich, Czech Republic).

We performed optical density (OD) analysis (25) of CSPG- and GFAP-stained slices from six brains chosen at random from among the wounded animals. All sections were examined at a final magnification of 40× with an Axioskop2 (Carl-Zeiss, Germany), and the images were captured under equal light conditions with a 14-bit CCD camera (AxioCam; Carl-Zeiss, Germany). The ODs were measured in the regions of interest (OD_{ROI}) and in a reference area (OD_{REF}). The relative ODs were calculated as follows: relative OD = 1 − (OD_{ROI}/OD_{REF}). The reference area was selected in the caudate putamen, and its OD was the same in the ipsilateral and contralateral hemispheres.

Statistical Analysis and Data Processing

The optical densitometry, TMA, and MR measurements were performed in the primary (S1) and secondary (S2) somatosensory cortices, in the primary auditory cortex (Au1), and in both the dorsal (AuD) and ventral (AuV) parts of the secondary auditory cortex. We divided the S1 area according to the distance from the injury site: the S1a region lay at a distance of 300–1000 μm laterally from the wound, and the S1b region at a distance of 1500–2000 μm laterally from the wound. A schematic drawing with the regions' placements is shown in Fig. 1a. The evaluated ROIs were positioned using a rat brain atlas (17) and T_2-weighted images (Fig. 1b). The size of the regions corresponded to that in the atlas, except for the S1 region, which was divided as described above.

The maps of the ADCs were calculated using the linear least-squares method. The ADC_W was assumed to be zero in pixels where the acquired data did not fit well to theoretical dependence (correlation coefficient < 0.2). These zero-values were ignored for statistical evaluations if they occurred in the ROI. Thereafter, the ADC_W maps were analyzed using ImageJ software (W. Rasband, NIH).

All data are presented as mean ± SEM; N represents the number of animals. Statistical analysis of the differences between groups was performed using the two-tailed Student's t-test (SigmaStat, SPSS Inc., Germany). The difference was considered significant with P-values < 0.05.

RESULTS

MR Measurements of ADC$_W$

T_2-weighted images were used to localize the wound (Fig. 1b). These T_2-weighted images also served to reveal potential undesirable postsurgical effects that could have affected the diffusion parameters (in two cases lateral ventricle enlargement was found, so these animals were eliminated from further data evaluation). Subsequently, DW images were acquired, and ADC$_W$ maps were calculated. For statistical processing, six regions (the same as for the evaluation of TMA measurements) were selected in the ipsilateral cortex, and six regions in the contralateral cortex (Fig. 1a). The evaluations were made in two adjacent slices, and their mean was used for further comparisons. The ROIs were placed both in the vicinity of the wound (in the S1a and S1b regions) and at a distance from the wound in the auditory cortex (AuD, Au1, and AuV). Details about the selection of ROIs are given in the Methods section.

We compared the mean values of ADC$_W$ in ROIs in the ipsilateral cortex of wounded animals with the mean values from corresponding regions in the contralateral hemisphere and in intact animals (controls). We did not find significant changes in ADC$_W$ in the contralateral cortex of wounded animals at 3, 7, or 21–35 days after injury when compared to control animals (ADC$_W$ = 0.65 ± 0.02 × 10^{-5} cm^{2}s^{-1} in the primary somatosensory cortex and ADC$_W$ = 0.67 ± 0.02 × 10^{-5} cm^{2}s^{-1} in the auditory cortex; N = 8). On the other hand, significant changes were observed in the whole ipsilateral cortex of wounded rats (Fig. 2). We found a significantly lower diffusion coefficient of water in the S1b, S2, AuD, Au1, and AuV regions of the wounded hemisphere at 3, 7, and 21–35 days after injury than in the contralateral hemisphere (ADC$_W$ ranged from 0.60 ± 0.02 × 10^{-5} cm^{2}s^{-1} in the S1b region to 0.56 ± 0.02 × 10^{-5} cm^{2}s^{-1} in the AuV region; N = 8). In the vicinity of the wound (S1a region), the changes in ADC$_W$ were not significant at 3 or 7 days post-wounding (ADC$_W$ = 0.59−0.61 × 10^{-5} cm^{2}s^{-1}); however, there was a significant difference 21–35 days after injury (ADC$_W$ = 0.58 ± 0.02 × 10^{-5} cm^{2}s^{-1}; N = 8). The data measured 7 days post-wounding are summarized in Fig. 3. In order to visualize the changes that occurred after the cortical stab wound, ADC$_W$ maps were converted to pseudocolor images (Fig. 2). The bottom part of Fig. 2 shows the decreased ADC$_W$ in the entire ipsilateral cortex of an injured rat brain 7 days post-wounding. Figure 2 further shows that the ADC$_W$ decrease corresponded to an increase in CSPG expression.

We conclude that a lower ADC$_W$ was found in those cortical regions that showed no changes in ECS volume fraction but did show an increase in CSPG expression, which presumably increased barriers not only for TMA$^+$ diffusion but also for that of water. There was a good correlation between the measurement of ADC$_{TMA}$ by the TMA method and the measurement of ADC$_W$ using DW-MRI.

In addition, we measured the directional dependence of ADC$_W$ in the cortex of control rats. For evaluation, we selected the S1, S2, and Au1 regions. Water diffusion in these regions can be described by a tensor. Using the tensors, which were related to the laboratory coordinates,
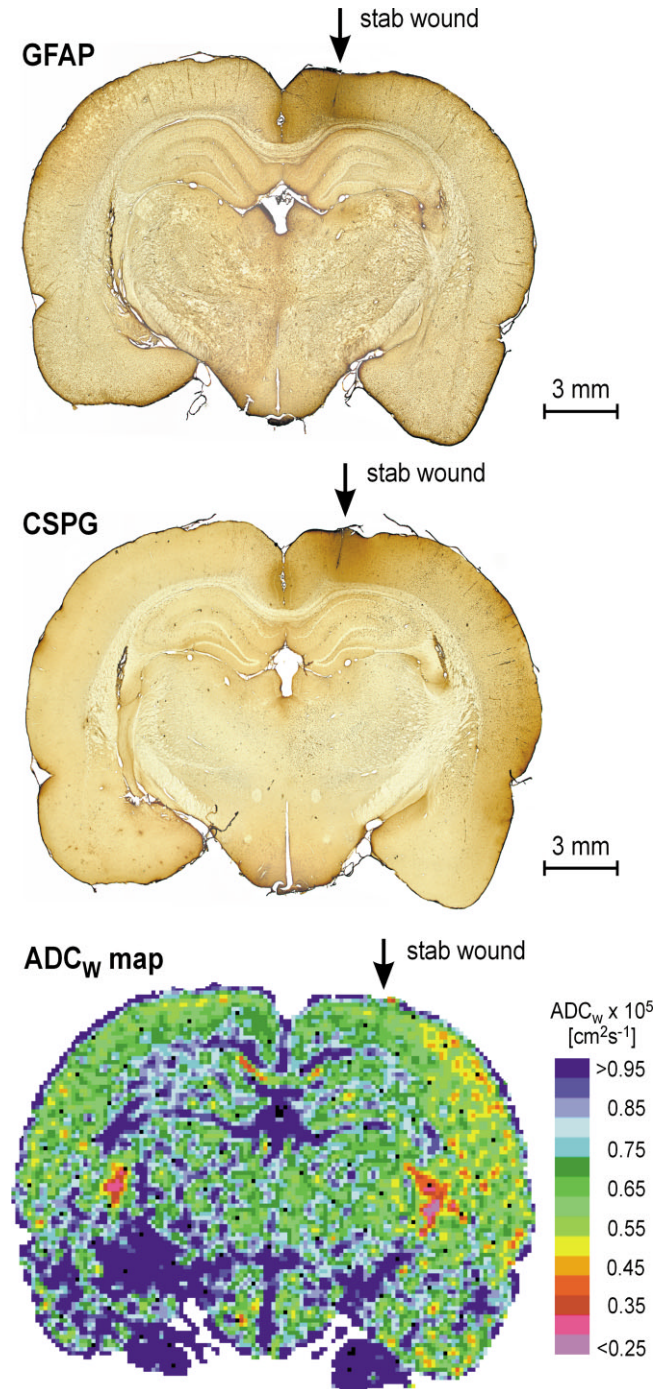

FIG. 2. The upper pictures show coronal rat brain sections stained for GFAP and CSPG. The results show a higher level of GFAP expression in the vicinity of the stab wound and a higher level of CSPG expression in the whole cortex of the injured hemisphere 7 days after injury. Both the GFAP and CSPG sections are from the same animal. The arrows indicate the site of the stab wound. ADC$_W$ map: The picture shows a typical ADC$_W$ map of an injured rat brain 7 days post-wounding. The scale on the right of the ADC$_W$ map shows the relation between the intervals of ADC$_W$ values and the colors used for visualization. The ADC$_W$ at 7 days post-wounding is significantly lower in the entire cortex of the wounded hemisphere, except in the area close to the wound (S1a).
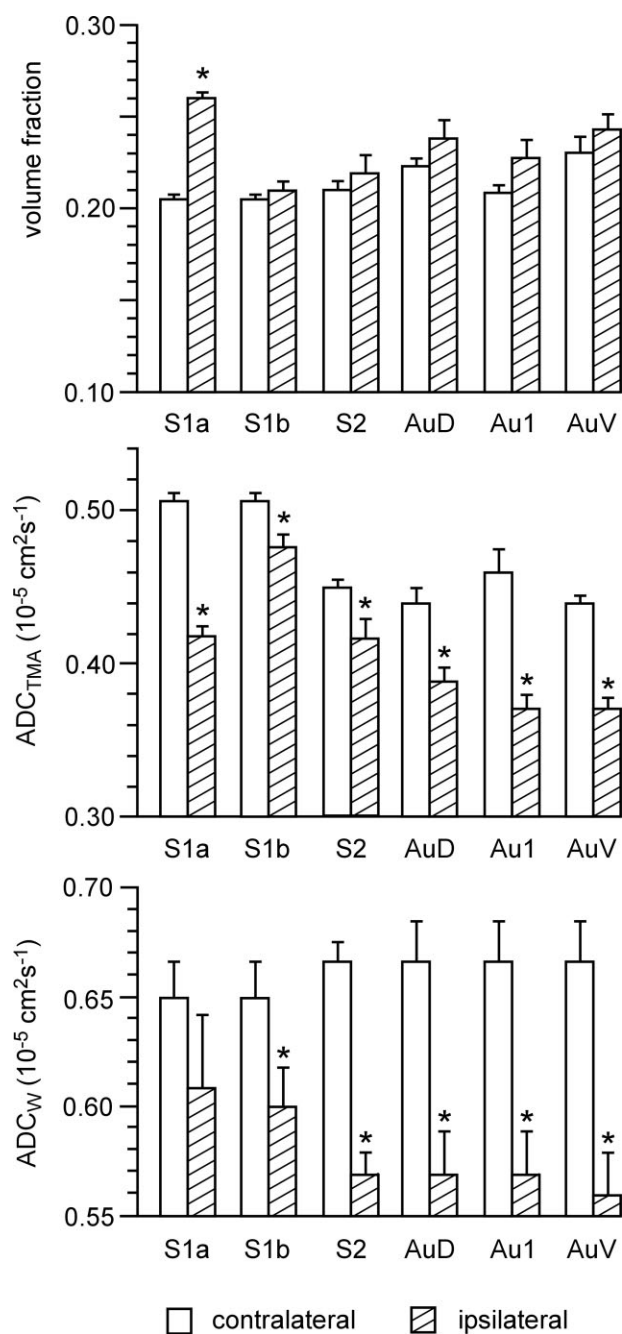
FIG. 3. The average values of the ECS volume fraction, ADC_{TMA}, and ADC_W in the cortex obtained at different distances from the wound 7 days post-lesion and in the hemisphere contralateral to the wound. All measurements were done along the *y*-axis in the S1a region (0.3–1.0 mm from the wound), the S1b region (1.5–2.0 mm from the wound), the S2, Au1, AuD, and AuV. Significant differences compared to controls are marked with asterisks (* = $P < 0.05$). All data are expressed as mean ± SEM; $N = 8$.

we calculated the components of ADC_W along the principal axes (corresponding to tensor matrix eigenvectors). At least two of the principal axes were the directions with the fastest and the slowest diffusion. We found that in the cortical regions S1, S2, and Au1 there was preferential diffusion in the direction of cortical columns. In the S1

and Au1 regions the principal axes coincided with the laboratory coordinates. Table 1 shows that in the S1 region, ADC_W was significantly higher (0.75 ± 0.02 × 10^{-5} cm^{2}s^{-1}; $N = 6$) along the *z*-axis than along the *x*- or *y*-axes. Similarly, there was a difference between the *x*-axis and the *y*-axis; however, the difference was less in this case. In the Au1 region, ADC_W was significantly higher (0.72 ± 0.02 × 10^{-5} cm^{2}s^{-1}; $N = 6$) along the *x*-axis when compared to ADC_W along the *z*- or *y*-axes. We did not find any difference between the diffusion coefficients measured along the *z*- and *y*-axes (Table 1).

TMA$^+$ Diffusion Measurements

The microelectrode tracks were located either in the vicinity of the injury (either 300–1000 μm (S1a) or 1500–2000 μm (S1b) lateral from the wound) or in the lateral part of the cortex (S2 and Au regions). In the primary somatosensory cortex of the hemisphere contralateral to the wound, the volume fraction, ADC_{TMA}, and nonspecific uptake were α = 0.21 ± 0.01, ADC_{TMA} = 0.51 ± 0.01 × 10^{-5} cm^{2}s^{-1}, and $k' = 3.1$ ± 0.2 × 10^{-3}s^{-1}; $N = 8$. These values in wounded animals did not significantly differ from those seen in intact brains in our previous studies (18,19) (Fig. 1c). In the region of the ipsilateral hemisphere with severe astrogliosis (<1000 μm distant from the wound, S1a region), the mean values of α were significantly higher 3 and 7 days post-wounding (α = 0.25–0.26), and the mean values of ADC_{TMA} were significantly lower 3, 7, and 21–35 days post-wounding (0.42–0.47 × 10^{-5} cm^{2}s^{-1}) than the values in the contralateral hemisphere (Figs. 1c and 3). The volume fraction (α) was not significantly increased in the rest of the ipsilateral cortex. In the region with mild astrogliosis (1500–2000 μm from the wound, S1b region) and in the auditory cortex (Au1, AuV), the mean values of ADC_{TMA} were significantly lower 7 days post-wounding (0.47 ± 0.01 × 10^{-5} cm^{2}s^{-1} in the S1b region and 0.37 ± 0.02 × 10^{-5} cm^{2}s^{-1} in the Au1 region; $N = 8$) than those in control animals or in the hemisphere contralateral to the wound (0.51 ± 0.01 × 10^{-5} cm^{2}s^{-1} in the S1b region and 0.46 ± 0.02 × 10^{-5} cm^{2}s^{-1} in the Au1 region; $N = 8$; Fig. 3).

The above diffusion coefficients were measured along the *y*-axis. Since there may be diffusion anisotropy in the cortex, we measured ADC_{TMA} in three directions in the somatosensory cortex (S1, S2) and in the auditory cortex (Au1, AuD, AuV) of control animals, and we found diffusion anisotropy in the S1, Au1, and AuV regions. The results from the S1 and Au1 regions are shown in Table 1. Preferential diffusion was found in the direction of cortical columns, i.e., along the *z*-axis in the S1 region and along the *x*-axis in the Au1 region. These values were higher than those along the remaining two perpendicular directions. Figure 4a shows the diffusion anisotropy at different cortical depths. Anisotropy can be illustrated by constructing surfaces that represent the probabilistic locations of molecules (ions) at a certain time τ after diffusion starts from a point source, as described by Nakada and Matsuzawa (26). The surfaces in Fig. 4b and c represent the locations 10 s after TMA$^+$ release from an iontophoretic micropipette. In a homogeneous tissue with isotropic dif-

Table 1
Diffusion Anisotropy in the Rat Cortex

Cortex region	x-Axis	y-Axis	z-Axis	N
S1				
$\quad$ADC$_{TMA}$	0.51 ± 0.01	0.49 ± 0.01	0.53 ± 0.01[b]	20
$\quad$ADC$_W$	0.59 ± 0.02	0.64 ± 0.01[a]	0.75 ± 0.02[a,b]	6
Au1				
$\quad$ADC$_{TMA}$	0.57 ± 0.03	0.47 ± 0.05	0.39 ± 0.01[a]	8
$\quad$ADC$_W$	0.72 ± 0.02	0.64 ± 0.02[a]	0.61 ± 0.01[a]	6

ADC$_W$ (ADC$_W$ × 10^5 cm^{2}s^{-1}) and ADC$_{TMA}$ (ADC$_{TMA}$ × 10^5 cm^{2}s^{-1}) were measured in intact animals along the x, y and z axes, (see Fig. 1), in the primary somatosensory cortex (S1) and in the primary auditory cortex (Au1). Significant differences ($P < 0.05$) between the TMA diffusion coefficients along different axes are marked ([a]compared to ADC$_x$, [b]compared to ADC$_y$). N represents the number of animals. The data are expressed as mean ± SEM.

fusion or in agar gel, the iso-concentration surface has the shape of a sphere, while in anisotropic tissue it has the shape of an ellipsoid (Au1). Diffusion anisotropy was still present in the auditory cortex (regions Au1 and AuV) 7 days after stab wounding. In the primary auditory cortex, the ADC$_{TMA}$ values along the x-axis decreased to 0.51 ± 0.01 × 10^{-5} cm^{2}s^{-1} ($N = 20$), and the values along the y- and z- axes to 0.37 ± 0.01 and 0.38 ± 0.01 × 10^{-5} cm^{2}s^{-1}, respectively ($N = 8$), at 7 days post-wounding.

Immunohistochemistry

After the MR and TMA diffusion measurements were performed, the animals were used for immunohistochemistry. Our immunohistochemical findings in the injured rat brain were in agreement with those of previous studies

(1,2). We found an increase in GFAP expression around the wound, and an increase in CSPG expression in the whole cortex ipsilateral to the wound. Both GFAP and CSPG changes persisted during the entire observation period (3–35 days post-lesion).

The level of GFAP expression in the injured hemisphere increased as early as 3 days post-lesion; it was most prominent at 7 days and thereafter slowly declined. GFAP expression was observed mainly at the injury site and was more intense in the immediate vicinity of the wound (Fig. 2). Severe astrogliosis was found in the cortical region at a distance of 300–1000 μm from the wound (S1a), while mild astrogliosis was found at a distance of 1500–2000 μm (S1b) from the wound (Fig. 5). In these regions, the relative OD of GFAP-stained slices was significantly higher than in
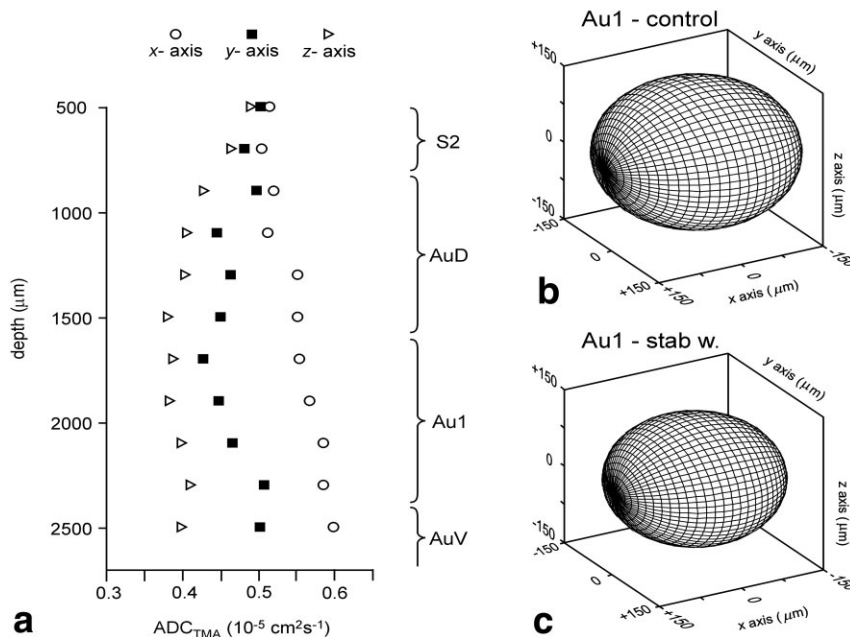

FIG. 4. Diffusion anisotropy in the auditory cortex. ADC$_{TMA}$ was measured in the S2 region and in the AuD, Au1, and AuV of intact rats ($N = 8$). **a:** The graph depicts the mean values of ADC$_{TMA}$ measured along the track in different axes. The diffusion anisotropy found in the auditory cortex of control rats persisted after injury. **b** and **c:** Diffusion spheres were calculated from measurements made in the Au1 of both (**b**) intact rats and (**c**) rats 7 days post-wounding; $N = 8$ in both groups. The probabilistic location of molecules diffusing from a certain point at time τ is an ellipsoidal surface. The surfaces show the probabilistic locations of TMA$^+$ 10 s after their release from an iontophoretic micropipette. The ellipsoidal surface illustrates anisotropic diffusion, and the smaller ellipsoid size reflects more hindered diffusion in the ipsilateral cortex of wounded animals.
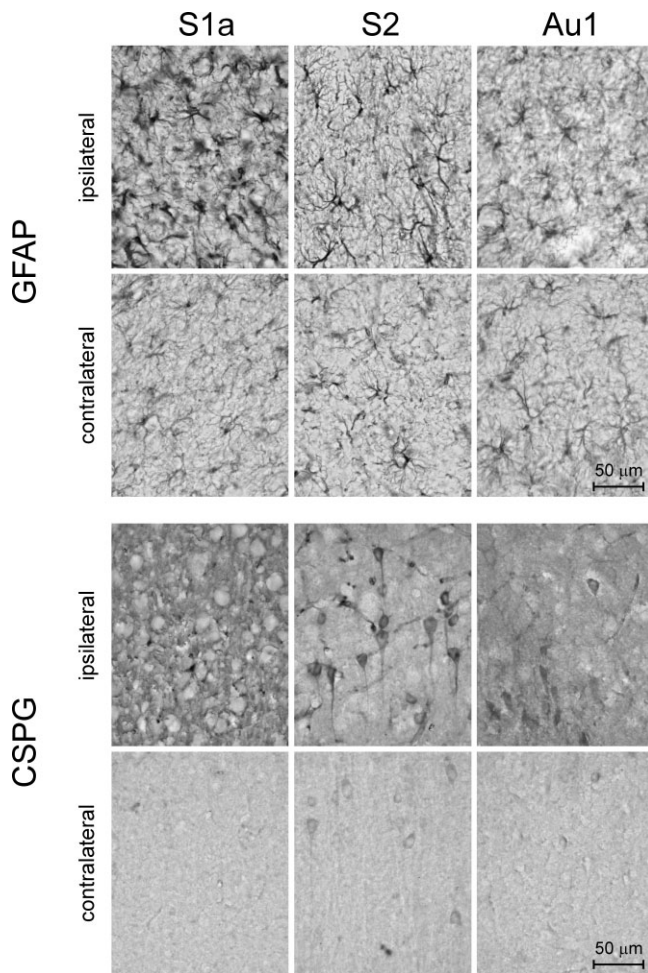
FIG. 5. Photomicrographs showing the differences in GFAP or CSPG expression between the wounded and contralateral hemispheres close to the wound (S1a) and at a distance from the wound (S2 and Au1) 7 days after injury. Note the astrogliosis in the S1a region and the prominent difference in CSPG expression between the hemispheres.

corresponding regions of the contralateral hemisphere (Fig. 6). In more distant areas of the ipsilateral cortex, we found only occasional hypertrophied astrocytes, and no change in the OD (Figs. 5 and 6) relative to the contralateral hemisphere.

The intensity of CSPG staining reached a peak as early as day 3 post-wounding and remained elevated thereafter. In contrast to GFAP, the area of elevated CSPG expression involved the whole ipsilateral cortex (Figs. 2 and 5), and the relative OD of CSPG staining was significantly increased in all selected ipsilateral cortical regions (S1a, S1b, S2, AuD, Au1, and AuD; Fig. 6) compared to the contralateral hemisphere. In the contralateral cortex, there was neither astrogliosis nor increased CSPG expression.

GFAP-stained sections were also used to identify the location of the electrodes after the TMA diffusion experiments.

DISCUSSION

A traumatic stab wound injury alters the ECS volume fraction in the vicinity of the wound. A significant increase

in α was found 3 and 7 days after lesion in the region with severe astrogliosis (S1a). Increased ECS volume has been described during various pathological states leading to cell death (27,28). Roitbak and Syková (2) proposed that in the first week after a stab wound, the volume fraction may be modified due to neuronal death, inflammation, the phagocytic activity of microglia, and the hypertrophy of astrocytes. The subsequent return of α to control values at 21–35 days post-wounding can be explained by the proliferation of astrocytes and the filling-up of the increased ECS volume resulting from the loss of myelin and neurons. In more distant parts of the ipsilateral cortex and in the contralateral cortex, we did not find any significant changes in ECS volume.

The ADC may also depend on the quantity and nature of diffusion barriers, which can affect the movement of diffusing particles. Such barriers in the brain are cell bodies and processes (in general, the cell membranes) and the molecules of the extracellular matrix (e.g., CSPG). In wounded animals, the ADC of TMA$^+$ was significantly decreased both in the vicinity of the wound (S1 region) and in the auditory cortex (Au1 and AuV). The decrease of $\mathrm{ADC_{TMA}}$ in the S1 region may be due to hypertrophied glial processes (see Fig. 5) or various macromolecules produced by glial cells and macrophages in the injured brain. The decrease in the auditory cortex, however, was related only to an increased density of extracellular matrix molecules (CSPG).
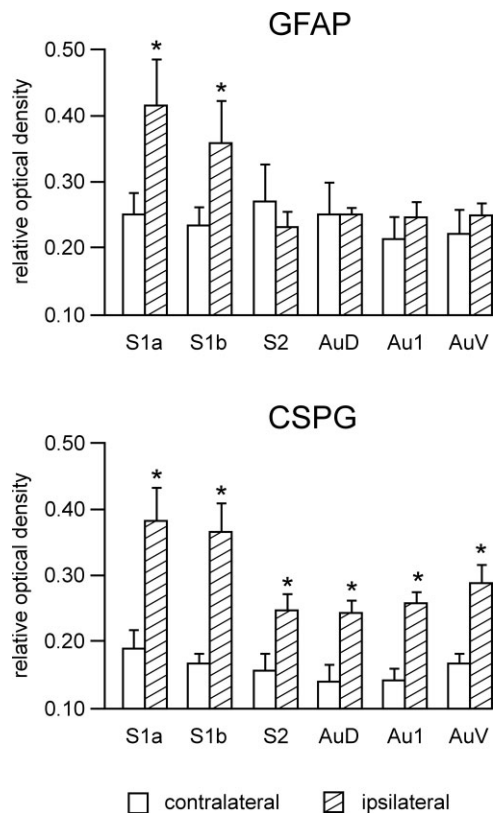

FIG. 6. Relative OD of GFAP and CSPG immunoreactivity in selected regions (see Fig. 1) of the injured and contralateral hemispheres. Significant differences between corresponding contralateral and ipsilateral regions are marked with asterisks (* = $P < 0.05$). All data are expressed as mean $\pm$ SEM; $N = 6$.

MR measurements revealed a significant ADC_W decrease in the entire ipsilateral part of the wounded cortex except for the region with an increased volume fraction (the S1a region at 3 and 7 days post-wounding). In this region there was no change in ADC_W, although ADC_{TMA} decreased. This apparent divergence between the results of the TMA and MR methods could be related to the fact that ADC_{TMA} and ADC_W are comprised of many components (15,29,30). In contrast to the TMA method, which measures ADC_{TMA} predominantly in the extracellular space, the MR method measures an effective ADC_W with contributions from the diffusion properties of multiple subcompartments, e.g., the extra- and intracellular spaces. If the volume ratio among the subcompartments in the tissue changes, the resulting ADC_W is also affected. In the regions without significant changes in ECS volume fraction (S1b, S2, and Au), there was a good correlation between DW-MRI and TMA diffusion measurements. In addition, changes in cell membrane permeability may influence ADC_W values (31). Conspicuous astrogliosis was not found in the ipsilateral auditory cortex (Au1 and AuV); however, there was a substantial increase in extracellular matrix molecules (CSPG), and the values of ADC_{TMA} and ADC_W were decreased. It is therefore evident that molecules of the extracellular matrix may significantly alter the ECS diffusion of TMA^+ as well as of water, without affecting the ECS volume fraction.

It is evident that in this study we measured the diffusion parameters in an injury model that results in substantial structural and diffusion changes over the course of several days. In stroke models, however, the situation is different since measurements are often done within minutes or hours after the onset of stroke, when cell swelling and edema formation are the most dramatic changes. In such acute pathologies a good correlation between changes in ADC_{TMA}, ADC_W, and ECS volume has been found (32).

Both the TMA and MR measurements in control animals revealed anisotropy in the primary somatosensory and auditory cortices (see Table 1 and Fig. 4). This has not been reported previously in studies using the TMA method (18,19). We found preferential diffusion in the direction of cortical columns. The structure of the tissue and the extent of myelination are the important factors that contribute to diffusion anisotropy (21,22). Prominent diffusion anisotropy was found after myelination and brain maturation (21). The decrease in the diffusion coefficients (ADC_{TMA} and ADC_W) observed in the auditory cortex after cortical stab wound was not accompanied by a loss of, or a change in anisotropy. This finding supports our opinion that diffusion in the Au region of wounded rats is hindered by the extracellular matrix rather than by other structural changes. The directional dependence of diffusion (ADC_W) has been previously reported in the rat cortex by other authors (33), correlating with our results. We measured the ADC of TMA^+ along three perpendicular axes, but this is not sufficient to completely characterize diffusion. The tensor of the diffusion coefficient consists of six independent components, so it would be necessary to measure diffusion in at least six noncolinear directions to describe the tensor nature of diffusion. However, in certain cases, when we select the "diffusion" directions according to the geometry of the tissue, we can directly measure the main

components (eigenvalues) of the tensor and ignore its non-diagonal components. For our measurements, we have chosen three such directions (laboratory coordinates) to comply with that condition in the cortical regions S1, AuD, Au1, and AuV. The apparent absence of anisotropy in ADC_{TMA} in the S2 region was probably caused by measurements in directions that did not correspond to tissue orientation (the laboratory coordinates were different from the principal axes). This fault may be corrected by simultaneous measurements made in more independent directions ($\geq$6), but in practice this is not feasible using the TMA method. Nevertheless, we also found diffusion anisotropy in the S2 region employing the MR method. We did not find changes in ADC_W anisotropy in cortical regions S1, S2, or Au1. However, ADC_{TMA} anisotropy was weak in the S1 area when compared to the auditory cortex (see Table 1). This divergence in the results of the two methods is probably caused by the different diffusion behavior of TMA^+ and water in brain tissue. In some cases different results have been found when the TMA^+ and MR methods were used for measuring diffusion anisotropy. In several studies, the authors reported diffusion anisotropy of water in unmyelinated tissue (34) or preceding myelination (35). Conversely, TMA^+ measurements demonstrated that the development of ADC_{TMA} diffusion anisotropy in the corpus callosum is associated with myelination (21).

The calculations of the ADC_W tensor were corrected for the effect of cross-terms (36). To verify the quality of our measurements, we evaluated ADC_W in phantoms placed on top of the rat's head, where the diffusion should be isotropic. We did not find significant differences along different directions. The maximal difference in ADC_W along two directions in the same phantom was <5%. These findings show that our measurements of ADC_W along different directions were not affected by any systematic error.

We conclude that traumatic injury is accompanied by changes in ADC_W in the whole ipsilateral cortex. The values of the ADCs measured by both the MR and TMA methods are closely correlated in regions in which the ECS volume fraction is not altered. We found that not only do cell swelling and changes in cell number or structure affect ADC_W, but also modifications in extracellular matrix composition can lead to changes in both ADC_W and ADC_{TMA}. Changes in diffusion barriers can occur in areas rather remote from the injury site, but where they may still affect synaptic as well as extrasynaptic "volume" transmission (14,15,37–40) and brain functions not directly related to the damaged areas.

REFERENCES

1. Norton WT, Aquino DA, Hosumi I, Chiu FC, Brosnan CF. Quantitative aspects of reactive gliosis: a review. Neurochem Res 1992;17:877–885.
2. Roitbak T, Syková E. Diffusion barriers evoked in the rat cortex by reactive astrogliosis. Glia 1999;28:40–48.
3. Bignami A, Dahl D. Astrocyte-specific protein and radial glia in the cerebral cortex of newborn rat. Nature 1974;252:55–56.
4. Mathewson AJ, Berry M. Observations on the astrocyte response to a cerebral stab wound in adult rats. Brain Res 1985;327:61–69.
5. Lindsay RM. Reactive gliosis. In: Fedoroff S, Vernadakis A, editors. Astrocytes. Cell biology and pathology of astrocytes. Orlando: Academic Press; 1986. p 231–262.

6. Hozumi I, Chiu F-C, Norton WT. Biochemical and immunocytochemical changes in glial fibrillary acidic protein after stab wounds. Brain Res 1990;524:64–71.

7. Hatten ME, Liem RKH, Shelanski ML, Mason CA. Astroglia in CNS injury. Glia 1991;4:233–243.

8. Vijayan VK, Lee YL, Eng LF. Increase in glial fibrillary acidic protein following neural trauma. Mol Chem Neuropathol 1990;13:107–118.

9. Levine J. Increased expression of the NG2 chondroitin-sulfate proteoglycan after brain injury. J Neurosci 1994;14:4716–4730.

10. Stichel CC, Kappler J, Junghans U, Koops A, Kresse H, Muller HW. Differential expression of the small chondroitin/dermatan sulfate proteoglycans decorin and biglycan after injury of the adult rat brain. Brain Res 1995;704:263–274.

11. Brückner G, Bringmann A, Härtig W, Köppe G, Delpech B, Brauer K. Acute and long-lasting changes in extracellular matrix chondroitin-sulphate proteoglycans induced by injection of chondroitinase ABC in the adult rat brain. Exp Brain Res 1998;121:300–310.

12. Nicholson C, Phillips JM. Ion diffusion modified by tortuosity and volume fraction in the extracellular microenvironment of the rat cerebellum. J Physiol (Lond) 1981;321:225–257.

13. Nicholson C, Syková E. Extracellular space structure revealed by diffusion analysis. Trends Neurosci 1998;21:207–215.

14. Syková E. The extracellular space in the CNS: its regulation, volume and geometry in normal and pathological neuronal function. Neuroscientist 1997;3:28–41.

15. Syková E. Glial diffusion barriers during aging and pathological states. Prog Brain Res 2001;132:339–363.

16. Le Bihan D, Basser PJ. Molecular diffusion and nuclear magnetic resonance. In: Le Bihan D, editor. Diffusion and perfusion magnetic resonance imaging: applications to functional MRI. New York: Raven Press; 1995. p 5–17.

17. Paxinos G, Watson C. The rat brain atlas in stereotaxic coordinates. Compact third edition. New York: Academic Press. 1996.

18. Lehmenkühler A, Syková E, Svoboda J, Zilles K, Nicholson C. Extracellular space parameters in the rat neocortex and subcortical white matter during postnatal development determined by diffusion analysis. Neuroscience 1993;55:339–351.

19. Voříšek I, Syková E. Ischemia-induced changes in the extracellular space diffussion parameters, K^+, and pH in the developing rat cortex and corpus callosum. J Cereb Blood Flow Metab 1997;17:191–203.

20. Mazel T, Šimonová Z, Syková E. Diffusion heterogeneity and anisotropy in rat hippocampus. NeuroReport 1998;9:1299–1304.

21. Voříšek I, Syková E. Evolution of anisotropic diffusion in the developing rat corpus callosum. J Neurophysiol 1997;78:912–919.

22. Rice ME, Okada YC, Nicholson C. Anisotropic and heterogeneous diffusion in the turtle cerebellum: implications for volume transmission. J Neurophysiol 1993;70:2035–2044.

23. Rice ME, Nicholson C. Diffusion characteristics and extracellular volume fraction during normoxia and hypoxia in slices of rat neostriatum. J Neurophysiol 1991;65:264–272.

24. Nicholson C. Quantitative analysis of extracellular space using the method of TMA^+ iontophoresis and the issue of TMA^+ uptake. Can J Physiol Pharmacol 1992;(Suppl)70:314–322.

25. Scheffler B, Faissner A, Beck H, Behle K, Wolf HK, Weistler OD, Blümcke I. Hippocampal loss of tenascin boundaries in Ammon's horn sclerosis. Glia 1997;19:35–46.

26. Nakada T, Matsuzawa H. Three-dimensional anisotropy contrast magnetic resonance imaging of the rats nervous system: MR angiography. Neurosci Res 1995;22:389–398.

27. Šimonová Z, Svoboda J, Orkand R, Bernard CCA, Lassmann H, Syková E. Changes of extracellular space volume and tortuosity in the spinal cord of Lewis rats with experimental autoimmune encephalomyelitis. Physiol Res 1996;45:11–22.

28. Syková E, Svoboda J, Šimonová Z, Lehmenkühler A, Lassmann H. X-irradiation-induced changes in the diffusion parameters of the developing rat brain. Neuroscience 1996;70:597–612.

29. Pfeuffer J, Provencher SW, Gruetter R. Water diffusion in rat brain in vivo as detected at very large *b* values is multicompartmental. MAGMA 1999;8:98–108.

30. Weglarz WP, Jasinski A, Pindel J, Adamek D, Kulinowski P, Skorka T. MR Microscopy studies of the appearance of the multiexponential diffusion in a rat spinal cord in vitro. In: Proceedings of the 9th Annual Meeting of ISMRM, Glasgow, Scotland, 2001. p 1517.

31. Helpern JA, Ordidge RJ, Knight RA. The effect of cell membrane water permeability on the apparent diffusion coefficient of water. In: Book of abstracts, 11th Annual Meeting of SMRM, Berlin, 1992. p 1201.

32. Van der Toorn A, Syková E, Dijkhuizen RM, Voříšek I, Vargová L, Škobisová E, Van Lookeren Campagne M, Reese T, Nicolay K. Dynamic changes in water ADC, energy metabolism, extracellular space volume, and tortuosity in neonatal rat brain during global ischemia. Magn Reson Med 1996;36:52–60.

33. Hoehn-Berlage M, Eis M, Schmitz B. Regional and directional anisotropy of apparent diffusion coefficient in rat brain. NMR Biomed 1999; 12:45–50.

34. Ono J, Harada K, Takahashi M, Maeda M, Ikenaka K, Sakurai K, Sakai N, Kagawa T, Fritz-Zieroth B, Nagai T, Nihei A, Hashimoto S, Okada S. Differentiation between dysmyelination and demyelination using magnetic resonance diffusional anisotropy. Brain Res 1995;671:141–148.

35. Wimberger DM, Roberts TP, Barkovich AJ, Prayer LM, Moseley ME, Kucharczyk J. Identification of "premyelination" by diffusion-weighted MRI. J Comput Assist Tomogr 1995;19:28–33.

36. Neeman M, Freyer JP, Sillerud LO. Effects of imaging gradients on diffusion measurements by MR imaging. In: Le Bihan D, editor. Diffusion and perfusion magnetic resonance imaging: applications to functional MRI. New York: Raven Press; 1995. p 73–76.

37. Chvátal A, Syková E. Glial influence on neuron signaling. Prog Brain Res 2000;125:199–216.

38. Fuxe K, Agnati LF. Volume transmission in the brain: novel mechanisms for neural transmission. New York: Raven Press; 1991.

39. Agnati LF, Zoli M, Stromberg I Fuxe K. Intercellular communication in the brain: wiring versus volume transmission. Neuroscience 1995;69: 711–726.

40. Zoli M, Jansson A, Syková E, Agnati LF, Fuxe K. Intercellular communication in the central nervous system. The emergence of the volume transmission concept and its relevance for neuropsychopharmacology. Trends Pharmacol Sci 1999;20:142–150.